Table III. Predicted Results for log W Using Neural Networks and Regression Analysis

	expt	est(NN)[a]	est(RA)[b]	ref
1. 4-heptanol	-1.40	-1.40	-1.61	11
2. menthone	-2.35	-2.72	-2.03	18
3. 1,1-diphenylethylene	-4.52	-5.23	-5.28	18
4. *p*-cresol	-0.81	-0.53	-0.44	25
5. testosterone	-4.08	-4.66	-4.49	22
6. 2,4,4'-PCB	-6.24	-5.96	-5.66	26
7. dexamethasone	-3.59	-3.47	-3.58	22
8. 4-chloronitrobenzene	-2.85	-1.83	-2.66	11
9. 2,5-PCB	-5.06	-5.75	-5.45	27
10. 2,6-PCB	-5.21	-5.52	-5.35	27
11. 2,4,6-PCB	-6.06	-6.24	-5.88	27
12. fluorene	-4.92	-4.43	-4.78	10
13. pyrene	-6.17	-6.04	-6.39	10
14. indan	-3.04	-3.10	-3.27	10
15. 3-methylpyridine	0.04	-0.01	-0.17	11
16. isoquinoline	-1.45	-1.11	-1.24	11
17. tetrahydrofuran	0.48	0.59	0.74	11
18. cortisone	-3.27	-2.95	-3.55	25
19. 2-naphthol	-2.25	-2.08	-1.61	25

[a] Estimation of log W using neural networks which gives a standard deviation 0.43. The standard deviation is 0.37 if we leave out the 4-chloronitrobenzene. [b] Estimation of log W using regression analysis which gives a standard deviation 0.36.

found to be superior to that obtained with the regression analysis approach, 0.30. The results clearly demonstrate that the neural network has captured the association between the selected properties of an organic compound and its aqueous solubility.

The trained neural network was tested on its ability to predict the aqueous solubility of an unknown set of organic compounds, that is, the compounds were not members of the original training set and indeed in some cases were quite unrelated to the original members. The test set should therefore provide a severe test of the neural network's predictive ability. Care should be taken in interpreting the results, however, since strictly the neural network should only be applied to predicting those compounds containing the particular substituents found in the training set. The results obtained are shown in Table III together with the values predicted by the regression analysis technique. Again the performance of the neural network is very satisfactory and compares favorably with that given by the regression analysis method. The neural network gives a predicted aqueous solubility superior to that obtained by regression analysis in 9 of the 19 cases. The poor value predicted for 4-chloronitrobenzene is probably due to the omission from the training set of any chloronitro compound which would reduce the credence attached to the predicted value.

In conclusion, a neural network model has been applied to the prediction of the aqueous solubility of organic compounds and the usefulness of the model clearly demonstrated. The predictive capability of neural networks has been demonstrated on a number of unknown organic compounds. It has been shown in this study that neural networks give a superior performance to that given by a regression analysis technique. While this work was in progress a paper was published[34] describing an application of the neural network approach to estimating quantitative structure–activity relationships. This work confirms the conclusions derived in this study that neural networks can determine such relationships with a performance exceeding that of linear multiregression analysis. Clearly, the neural network approach would seem to have great potential for determining quantitative structure–activity relationships and as such be a valuable tool for the medicinal chemist.

Supplementary Material Available: Listing of complete experimental and estimated log W values (6 pages). Ordering information is given on any current masthead page.

(34) Aoyoma, T.; Suzuki, Y.; Ichikawa, H. *J. Med. Chem.* **1990**, *33*, 2583.

Computational Studies on FK506: Conformational Search and Molecular Dynamics Simulation in Water

Julianto Pranata and William L. Jorgensen*

Contribution from the Department of Chemistry, Yale University, New Haven, Connecticut 06511.
Received May 6, 1991

Abstract: Computational investigations have been undertaken to elucidate the conformational characteristics and the hydration of the immunosuppresant FK506. The calculations made use of the AMBER/OPLS molecular mechanics force field, augmented with some newly developed parameters particularly for the α-ketoamide torsion. A conformational search on FK506 using an internal coordinate Monte Carlo method found 21 distinct energy minima within 12 kcal/mol of the lowest energy structure. The minima include structures with both cis and trans conformations of the amide bond. A 200-ps molecular dynamics simulation in water then provided information on the dynamical behavior of the cis isomer of FK506 as well as its hydration. Two conformations of the macrocyclic ring are sampled during the simulation, and some exocyclic groups undergo rapid conformational changes. Considerable flexibility is also observed near the amide functionality, which is in the binding region of FK506. The hydration of FK506 shows interesting variations owing to differences in the steric environments of potential hydrogen-bonding sites. In the critical binding region, there are on average 5 hydrogen bonds between water molecules and FK506.

FK506, rapamycin, and cyclosporin A (CsA) are immunosuppresive agents that act by blocking the signal transduction pathways that lead to T lymphocyte activation.[1] FK506 and rapamycin are structurally similar and appear to bind to the same receptor, FKBP,[2] while the structurally unrelated CsA, a cyclic undecapeptide, binds to a different receptor, cyclophilin.[3] Both receptors have been shown to be peptidyl-prolyl cis–trans isomerases (rotamases).[4,5] FK506 and rapamycin inhibit the rotamase activity of FKBP, but not of cyclophilin; likewise CsA inhibits the rotamase activity of cyclophilin, but not of FKBP.[4]

(1) Schreiber, S. L. *Science* **1991**, *251*, 283.
(2) Bierer, B. E.; Mattila, P. S.; Standaert, R. F.; Herzenberg, L. A.; Burakoff, S. J.; Crabtree, G.; Schreiber, S. L. *Proc. Natl. Acad. Sci. U.S.A.* **1990**, *87*, 9231. Dumont, F. J.; Melino, M. R.; Staruch, M. J.; Koprak, S. L.; Fischer, P. A.; Sigal, N. H. *J. Immunol.* **1990**, *144*, 1418. Fretz, H.; Albers, M. W.; Galat, A.; Standaert, R. F.; Lane, W. S.; Burakoff, S. J.; Bierer, B. E.; Schreiber, S. L. *J. Am. Chem. Soc.* **1991**, *113*, 1409.
(3) Handschumacher, R. E.; Harding, M. W.; Rice, J.; Drugge, R. J.; Speicher, D. W. *Science* **1984**, *226*, 544. Handschumacher, R. E.; Harding, M. W. *Transplantation* **1988**, *46*, 29S.
(4) Harding, M. W.; Galat, A.; Uehling, D. E.; Schreiber, S. L. *Nature* **1989**, *341*, 758. Siekierka, J. J.; Hung, S. H. Y.; Poe, M.; Lin, C. S.; Sigal, N. H. *Nature* **1989**, *341*, 755.
(5) Fischer, G.; Wittmann-Liebold, B.; Lang, K.; Kiefhaber, T.; Schmid, F. X. *Nature* **1989**, *226*, 544. Takahashi, N.; Hayano, T.; Suzuki, M. *Nature* **1989**, *226*, 473.

0002-7863/91/1513-9483$02.50/0

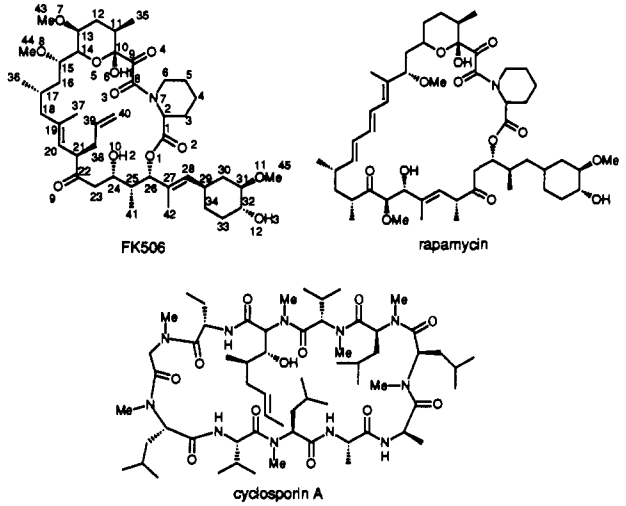

Crystal structures of all three immunosuppresants have been reported.[6-8] In addition, NMR data have been used to deduce the structure of CsA in a variety of solvents.[6,9] The solution-phase structure for FK506 in $CDCl_3$ has also been examined.[10]

Schreiber and co-workers have investigated the inhibition of FKBP rotamase activity by FK506.[11] The immunosuppresant with ^{13}C labels at C8 and C9 was synthesized[12] and used to probe the binding process. ^{13}C NMR of the enzyme–inhibitor complex shows no evidence for the existence of a tetrahedral adduct at either C8 or C9. Thus, the mechanism for rotamase activity does not involve the formation of a tetrahedral intermediate; rather, a mechanism was proposed which features a twisted amide bond in the transition state. The α-ketoamide functionality in FK506 (and rapamycin) has an orthogonal orientation in the crystal structure[7,8] and serves as a surrogate for the twisted amide bond. Thus, by acting as a transition-state analogue, FK506 potently inhibits rotamase activity.

Interestingly, the NMR of FK506 in solution shows the existence of two isomers, attributed to the cis and trans conformations for the amide bond in a 2:1 ratio.[10,11] It has recently been determined by X-ray crystallography that the trans isomer is bound to FKBP,[13] though only the cis isomer is observed in the crystal structure of isolated FK506.[7] For CsA, both in the crystal and in solution the molecule has a cis peptide bond between residues MeLeu 9 and MeLeu 10.[6,9] However, there is evidence that CsA bound to cyclophilin also adopts a trans conformation for this bond.[14]

On the computational side, Lautz et al. have reported molecular dynamics simulations of CsA in water, CCl_4, and the crystalline environment.[15] The focus was on comparisons with experimental structural data and medium effects on the conformation of CsA. However, the 40–50-ps durations for the simulations severely limited the conformational sampling.

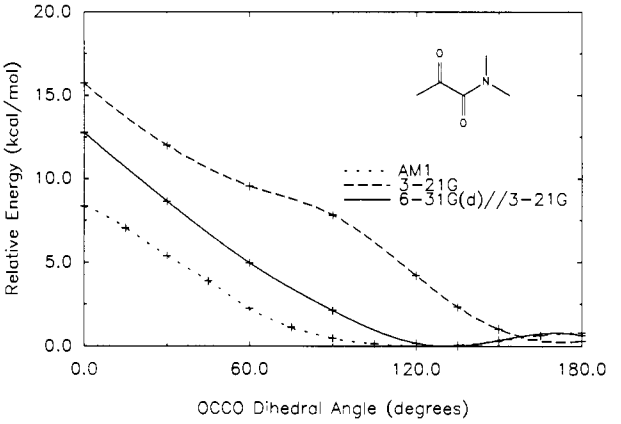

Figure 1. Torsional profiles of *N*,*N*-dimethyl-α-ketopropanamide from molecular orbital calculations.

We are interested in investigating the structural and energetic aspects of the binding of immunosuppresants and substrates to FKBP. The initial efforts, described here, addressed the development of needed force-field parameters for FK506, conformational search for low-energy structures in the absence of solvent, and characterization of the hydration and internal motions of FK506 through a 200-ps molecular dynamics simulation in water.

Parameter Development

A principal difficulty in performing computations on molecules like FK506 is the lack of appropriate molecular mechanics parameters. For proteins and nucleic acids, a variety of standard parameter sets are available, e.g., AMBER[16] or CHARMm.[17] However, FK506 contains functionalities not found in peptides or nucleotides. In particular, an accurate description of the α-ketoamide torsion is required, in view of its importance in the binding process.[11]

Where available, parameters and potential functions from the AMBER force field were used for bonded interactions (bond stretches, bends, and torsions, including improper torsions).[16] The OPLS parameters and functions were used for nonbonded interactions.[18] Some parameters were added to the AMBER set on the basis of existing parameters for similar functional groups. Appropriate parameters were not found for some torsions involving esters, ketones, and olefins. Parameters appropriate for an ester group were recently developed by Charifson et al.[19] and were used in the present work. Other torsional parameters were obtained by fitting to ab initio torsional profiles calculated by Wiberg and co-workers.[20] A united-atom model has been here for CH_n units, otherwise all atoms are explicitly represented.

As mentioned above, the α-ketoamide torsion is particularly important, and the parameters for this functionality were developed with the aid of quantum mechanical calculations. *N*,*N*-Dimethyl-α-ketopropanamide was chosen as a model system, and the torsional profile for the bond between the two carbonyl carbons was computed using semiempirical (AM1)[21,22] and ab initio

(6) Loosli, H. R.; Kessler, H.; Oschkinat, H.; Weber, H. P.; Petcher, T. J.; Widmer, A. *Helv. Chim. Acta* **1985**, *68*, 682.
(7) Tanaka, H.; Kuroda, A.; Marusawa, H.; Hatanaka, H.; Kino, T.; Goto, T.; Hashimoto, M.; Taga, T. *J. Am. Chem. Soc.* **1987**, *109*, 5031. Taga, T.; Tanaka, H.; Goto, T.; Tada, S. *Acta Crystallogr.* **1987**, *C43*, 751.
(8) Swindells. D. C. N.; White, P. S.; Findlay, J. A. *Can. J. Chem.* **1978**. *56*, 2491.
(9) Kessler, H.; Oschkinat, H.; Loosli, H. R. *Helv. Chim. Acta* **1985**, *68*, 661. Kessler, H.; Köck, M.; Wein, T.; Gehrke, M. *Helv. Chim. Acta* **1990**, *73*, 1818.
(10) Karuso, P.; Kessler, H.; Mierke, D. F. *J. Am. Chem. Soc.* **1990**, *112*, 9434.
(11) Rosen, M. K.; Standaert, R. F.; Galat, A.; Nakatsuka, M.; Schreiber, S. L. *Science* **1990**, *248*, 863.
(12) Nakatsuka, M.; Ragan, J. A.; Sammakia, T.; Smith, D. B.; Uehling, D. E.; Schreiber, S. L. *J. Am. Chem. Soc.* **1990**, *112*, 5583.
(13) Van Duyne, G. D.; Standaert, R. F.; Karplus, P. A.; Schreiber, S. L.; Clardy, J. *Science* **1991**, *252*, 839.
(14) Fesik, S. W.; Gampe, R. T., Jr.; Holzman, T. F.; Egan, D. A.; Edalji, R.; Luly, J. R.; Simmer, R.; Helfrich, R.; Kishore, V.; Rich, D. H. *Science* **1990**, *250*, 1406.
(15) Lautz, J.; Kessler, H.; van Gunsteren, W. F.; Weber, H. P.; Wenger, R. M. *Biopolymers* **1990**, *29*, 1669. Lautz, J.; Kessler, A.; Kaptein, R.; van Gunsteren, W. F. *J. Computer-Aided Mol. Design* **1987**, *1*, 219.
(16) Weiner, S. J.; Kollman, P. A.; Case, D. A.; Singh, U. C.; Ghio, C.; Alagona. G.; Profeta, S., Jr.; Weiner, P. *J. Am. Chem. Soc.* **1984**, *106*, 765. Weiner, S. J.; Kollman, P. A.; Nguyen, D. T.; Case, D. A. *J. Comp. Chem.* **1986**, *7*, 230.
(17) Brooks, B. R.; Bruccoleri, R. E.; Olafson, B. D.; States, D. J.; Swaminathan, S.; Karplus, M. *J. Comp. Chem.* **1983**, *4*, 187. Nilsson, L.; Karplus, M. *J. Comp. Chem.* **1986**, *7*, 591.
(18) Jorgensen, W. L.; Tirado-Rives, J. *J. Am. Chem. Soc.* **1988**, *110*, 1657. Jorgensen, W. L.; Briggs, J. M.; Conteras, M. L. *J. Phys. Chem.* **1990**, *94*, 1683.
(19) Charifson, P. S.; Hiskey, R. G.; Pedersen, L. G. *J. Comp. Chem.* **1990**, *10*, 1181.
(20) Wiberg, K. B.; Martin, E. *J. Am. Chem. Soc.* **1985**, *107*, 5035. Wiberg, K. B. *J. Am. Chem. Soc.* **1986**, *108*, 5817. Wiberg, K. B.; Laidig, K. E. *J. Am. Chem. Soc.* **1987**, *109*, 5935.
(21) Dewar, M. J. S.; Zoebisch, E. G.; Healy, E. F.; Stewart, J. J. P. *J. Am. Chem. Soc.* **1985**, *107*, 3902.
(22) AM1 calculations were performed using the MOPAC program. Stewart, J. J. P. MOPAC 5.0; QCPE Program No. 455; Indiana University, Bloomington, IN.

Table I. New AMBER Torsion Parameters

torsion	$V_1/2$	γ	$V_2/2$	γ	$V_3/2$	γ
			Ester			
CH—C(=O)—O—C[a]	2.545	0.0				
O=C—O—C[a]			4.150	180.0		
O—C(=O)—CH—X	0.470	0.0	0.500	180.0		
			Ketone			
C—C(=O)—C—X	0.203	0.0	0.230	180.0		
C—C(=O)—CH—X	0.305	0.0	0.345	180.0		
C—C(=O)—CH_2—X	0.610	0.0	0.690	180.0		
			Olefin			
X—C=C—X			7.500	180.0		
C=CH—CH_2—X	0.700	180.0			1.100	180.0
C=CH—CH—X	0.350	180.0			0.550	180.0
C=C—CH_2—X	0.350	180.0			0.550	180.0
C=C—CH—X	0.175	180.0			0.275	180.0
C—C(=C)—CH_2—X	0.350	0.0			0.550	0.0
C—C(=C)—CH—X	0.175	0.0			0.275	0.0
			α-Ketoamide			
O=C—C=O	0.12	180.0	0.42	180.0		
O=C—C—N	0.12	0.0	0.42	180.0		
C—C—C=O	0.12	0.0	0.42	180.0		
C—C—C—N	0.12	180.0	0.42	180.0		

[a] Reference 19.

(HF/3-21G and HF/6-31G(d)//3-21G)[23,24] molecular orbital calculations. The results are shown in Figure 1. Both the AM1 and 6-31G(d) calculations predict a nonplanar minimum, although the barrier at the anti conformation is quite low. For AM1, the minimum occurs at 124° and the height for the anti barrier is 0.79 kcal/mol, while the corresponding values from the 6-31G(d) calculations are 135° and 0.65 kcal/mol. However, the 3-21G results appear to overestimate the stability of the anti conformation, making it the minimum. In the crystal structures, the α-ketoamide functionality in both FK506 and rapamycin has an orthogonal orientation.[7,8] The same trend is observed in other molecules when this functionality is doubly substituted at the nitrogen; e.g., tetramethyloxamide is twisted by 71°.[25]

AMBER-type parameters were then obtained by fitting to the 6-31G(d) torsional profile. The fitting took into account the substantial nonbonded interactions in this molecule. In fact, it turned out that the nonbonded (i.e., steric) interactions are solely responsible for the nonplanarity of the system; there is nothing unusual about the torsional parameters that are reported in Table I.

As a test of the new parameters, they were incorporated into AMBER and used to compute the torsional profile of a non-macrocyclic fragment of the FK506 structure. This is compared to the profile computed using AM1 in Figure 2. Although the AMBER profile has a shallower minimum, the difference is not great, and the two profiles have the same overall shape. The minimum in the results with AMBER occurs at −108°, compared to −96° with AM1, while in the crystal structure of FK506 this torsional angle is −89°.[7]

All of the torsional parameters added to the AMBER set for the purpose of this work are presented in Table I. In addition, a complete listing of the parameters for FK506 is given in the Supplementary Material. The same parameters were used for the conformational search and molecular dynamics.

Conformation Search

Procedure. A fairly extensive search for the conformational minima of FK506 in the ideal gas phase was performed using an internal coordinate Monte Carlo method.[26] The focus was on the conformation of the 21-membered macrocycle. No search was conducted which involved variations of the exocyclic torsions. Also excluded were torsions within six-membered rings, namely those for the C2–N7, C10–O5, and O5–C14 bonds, as well as the double bond (C19–C20). The remaining 17 dihedral angles were randomly varied; however, O1–C1 was defined as the ring-closure bond, so its torsion and the torsions around the two adjacent bonds (C1–C2 and C26–O1) were not explicitly varied. Of course, no constraints were applied in the subsequent energy minimizations.

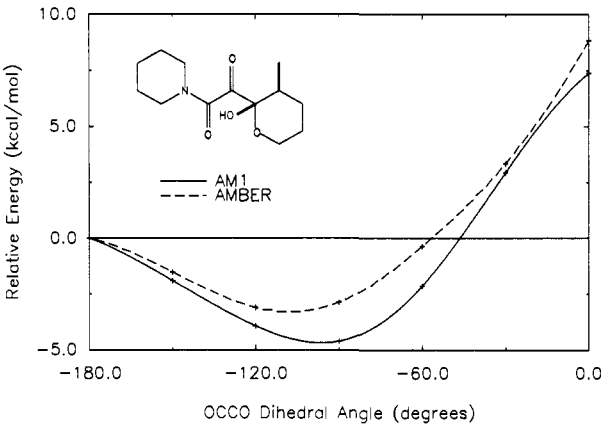

Figure 2. Torsional profiles of a fragment of FK506.

The starting structure for the search was obtained from the X-ray crystal structure.[7] Initially, all hydrogens bound to carbons were removed, resulting in representation of FK506 as 60 explicit atoms. This structure was energy minimized, and the resulting structure was used to start the conformational search. The RMS deviation between the actual X-ray structure and the energy-minimized form is only 0.48 Å. The only significant change is the formation of a hydrogen bond between O6–H1 and O4 that is not in the crystal structure (vide infra). A total of 8499 structures were generated using a random walk procedure; these were initially minimized to a root mean square gradient of 1 kJ/(mol·Å) (=0.239 kcal/(mol·Å)). Nonduplicate structures whose energies were within 50 kJ/mol (=12 kcal/mol) above the lowest energy minimum were saved. This resulted in 28 structures which were further minimized to a root mean square gradient of

(23) Hehre, W. J.; Radom, L.; Schleyer, P. v. R.; Pople, J. A. *Ab Initio Molecular Orbital Theory*; Wiley: New York, 1986.

(24) Ab initio calculations were performed using the GAUSSIAN 90 programs. Frisch, M. J.; Head-Gordon, M.; Trucks, G. W.; Foresman, J. B.; Schlegel, H. B.; Raghavachari, K.; Robb, M. A.; Binkley, J. S.; Gonzalez, C.; Defrees, D. J.; Fox, D. J.; Whiteside, R. A.; Seeger, R.; Melius, R.; Baker, J.; Martin, R. L.; Kahn, L. R.; Stewart, J. J. P.; Topiol, S.; Pople, J. A. GAUSSIAN 90 Revision F; Gaussian Inc.: Pittsburgh, PA, 1990.

(25) Adiwidjaja, G.; Voss, J. *Chem. Ber.* **1977**, *110*, 1159.

(26) Chang, G.; Guida, W. C.; Still, W. C. *J. Am. Chem. Soc.* **1989**, *111*, 4379.

Table II. Values of Macrocyclic Dihedral Angles (deg) in the Conformations Found in the Monte Carlo Search and in the X-ray Structure

	conformation								
dihedral angle	1	2	3	4	5	6	7	8	9
O1C1C2N7[b]	43	86	−168	179	87	91	−179	−178	−165
C1C2N7C8[c]	−95	−93	−100	−100	−101	−95	−100	−99	−100
C2N7C8C9	165	0	−2	0	−5	1	−3	2	−4
N7C8C9C10	167	−63	−105	−115	−96	−68	−99	−87	−104
C8C9C10O5	75	90	65	55	72	91	68	81	68
C9C10O5C14[c]	177	179	173	169	178	178	179	175	177
C10O5C14C15[c]	−177	−179	−176	−176	−177	−176	−177	−175	−177
O5C14C15C16	75	86	62	49	76	85	78	75	92
C14C15C16C17	57	65	65	52	68	68	60	89	−78
C15C16C17C18	−168	−172	−151	−159	−169	−170	−179	−170	−159
C16C17C18C19	60	66	−63	155	70	74	60	−56	167
C17C18C19C20	−107	−121	71	130	−123	−119	−126	16	−67
C18C19C20C21[c]	176	−179	175	175	−177	−176	−176	171	179
C19C20C21C22	−115	−123	−142	−115	−124	−110	−124	−118	−129
C20C21C22C23	73	106	83	101	122	−39	138	−48	101
C21C22C23C24	−152	−99	178	−120	148	122	−157	−148	174
C22C23C24C25	−58	−65	146	172	172	175	169	−64	169
C23C24C25C26	−71	−145	−61	−69	−84	−163	−69	−65	−67
C24C25C26O1	−40	−56	−23	−42	45	−55	−37	−24	−23
C25C26O1C1[b]	−154	−154	−147	−146	−147	−153	−149	−155	−147
C26O1C1C2[b]	−175	−169	−162	−177	−160	−169	−176	−171	−165
energy[d]	17.6	20.6	23.3	23.9	24.4	24.5	25.7	25.9	26.4

[a] After minimization. [b] O1C1 is defined as the ring closure bond, thus these dihedral angles are not explicitly included in the search. [c] These

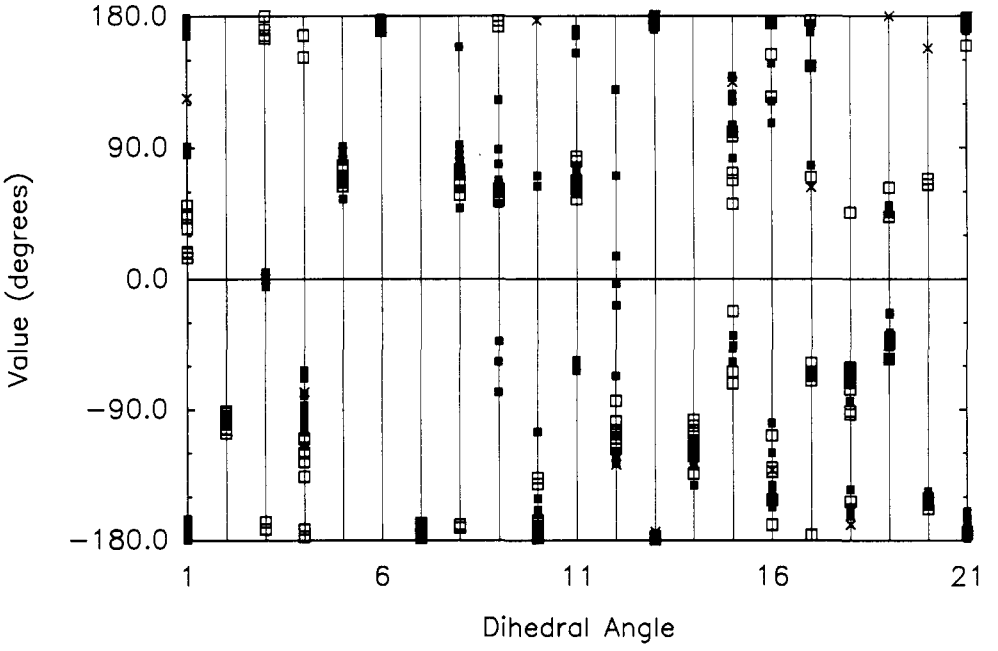

Figure 3. Distribution of macrocyclic dihedral angles in the 21 structures found in the Monte Carlo search. Open squares are for trans amide isomers and filled squares for cis. Also shown are the dihedral angles of the X-ray structure after minimization (×). The numbers of the dihedral angles on the abscissa correspond to the list in Table II.

0.1 kJ/(mol·Å). After elimination of duplicates and high-energy structures, 21 distinct minima were found.

The energy minimizations were performed using a dielectric constant of 1.0 and a cutoff distance of 9.0 Å for both van der Waals and electrostatic interactions. The calculations were performed with the BATCHMIN program, Version 2.7, on a DEC VaxStation 3500 minicomputer.[27]

Results. The dihedral angles for the macrocyclic ring in the 21 conformational minima found during the search are listed in Table II along with relative potential energies. A distribution of the dihedral angles is represented in Figure 3. Both Table II and Figure 3 also contain data for the conformation from the X-ray structure after minimization. The 21 energy minima include both trans and cis amide isomers. Stereopictures of the lowest energy trans (**1**) and cis (**2**) forms are shown in Figure 4, along with the energy minimized X-ray structure; corresponding pictures and coordinates for all 22 structures are available in the Supplementary Material.

It is emphasized that we did not attempt to locate *all* the conformational minima of FK506; to do so would have necessitated a much longer search as well as the inclusion of variations of the exocyclic and six-membered-ring torsions. However, the 21 structures may be expected to be representative of the low-energy conformations of FK506.

All 21 structures are reasonable in that no bonds or angles are unduly strained. Somewhat surprisingly, the X-ray crystal structure is not among these 21 structures. Its energy, or rather, the energy of the minimum closest to it, is 14.7 kcal/mol above the energy of the lowest minimum found. A minimization was

(27) BATCHMIN is the noninteractive part of the MACROMODEL molecular modeling program. Mohamadi, F.; Richards, N. G. J.; Guida, W. C.; Liskamp, R.; Lipton, M.; Caufield, C.; Chang, G.; Hendrickson, T.; Still, W. C. *J. Comp. Chem.* **1990**, *11*, 440.

conformation												
10	**11**	**12**	**13**	**14**	**15**	**16**	**17**	**18**	**19**	**20**	**21**	X-ray[a]
51	176	19	35	45	167	18	−172	173	19	89	15	124
−95	−98	−98	−106	−103	−97	−91	−99	−99	−92	−98	−94	−93
167	2	180	−172	−167	5	167	−2	−2	171	−3	167	0
152	−90	−172	−110	−120	−80	−136	−79	−115	−126	−88	−177	−78
78	72	69	75	69	84	67	89	72	64	81	69	87
175	172	174	170	173	175	172	176	176	170	177	173	176
−178	−170	−175	−168	−169	−177	−174	−169	−177	−173	−174	−177	−176
66	159	72	−169	−171	76	66	78	86	58	82	74	80
60	−43	57	177	173	79	60	123	−57	54	65	62	63
−170	−105	−166	−137	−141	−162	−178	64	71	−170	−177	−174	177
62	77	67	81	84	−57	63	72	171	55	65	68	63
−113	−127	−105	−98	−84	−3	−104	−108	−18	−113	−122	−117	−128
178	−175	−179	176	180	178	−177	180	177	174	−177	−179	−174
−118	−120	−106	−122	−97	−112	−101	−115	−122	−134	−117	−117	−122
68	139	−64	52	−72	−57	−22	−46	105	98	127	101	135
−169	−154	125	175	154	107	−133	−142	−142	−130	−147	−108	−132
−58	173	146	−70	70	78	−176	−68	173	177	172	−64	63
−68	−73	−76	−93	−153	−157	46	−63	−68	−61	−162	−91	−169
−40	−41	−45	−55	−55	−47	43	−23	−38	63	51	−45	180
−151	−149	−152	−151	−158	−154	69	−155	−150	65	−155	−155	158
−174	−178	179	178	177	−170	173	−167	177	160	−165	175	173
26.4	26.7	26.7	26.8	27.0	27.4	27.4	27.5	27.7	28.2	28.3	28.3	32.3

dihedral angles are not included in the search. [d] Energies in kcal/mol.

also carried out starting with the geometry of bound FK506 obtained from the X-ray crystal structure of its complex with FKBP.[13] The resultant structure had an energy 21.5 kcal/mol above the lowest energy minimum.

Interestingly, the cis isomers appear to favor a perpendicular orientation of the adjacent carbonyl groups (C8–C9 dihedral angle), while the trans isomers are more tolerant of an anti orientation in this position. Another noticeable difference is that the conformation about the C1–C2 bond is always gauche-like in the trans isomers; it is usually anti in the cis. These trends, of course, only reflect the results for the 21 structures. However, these torsions are in the binding region of FK506, and the tendencies they show may be important in view of the observation that only the trans isomer is bound to FKBP.[13] No other trends are strikingly apparent which differentiate the cis and trans isomers.

Not surprisingly, the four torsions excluded from the search (those around the C2–N7, C10–O5, O5–C14, and C19–C20 bonds) remain in their initial conformation (Figure 3). Three other torsions also show no tendency for variations, namely those around the C9–C10, C20–C21, and O1–C1 bonds. The anti orientation for the last torsion means that the ester is always in the *Z* form. Most of the rest of the torsions are clustered into easily identifiable gauche and anti conformations. Of course, the torsions flanking the double bond (C18–C19 and C20–C21) are expected to cluster around skew and syn conformations instead, and they do, except that C20–C21 is a torsion that remains skew in all 21 structures. The torsions flanking the isolated keto group (C21–C22 and C22–C23) show a rather large spread of values, and do not appear to be easily categorized into gauche or anti conformations.

A major reason for the absence of the X-ray crystal structure from the set is the presence of intramolecular hydrogen bonds. The actual X-ray structure does not have any intramolecular hydrogen bonds, but one (O6—H1···O4) was formed upon energy minimization (Figure 4). This hydrogen bond is present in all the other structures; furthermore, 16 of these structures have additional hydrogen bonds involving O10–H2 as a donor (Table III). In the actual crystal structure, O10–H2 acts as an intermolecular hydrogen bond donor to O9 of a neighboring molecule.[7] In addition, one water molecule was located in the crystal which forms the hydrogen bonds O6—H1···O(W) and O(W)—H···O4, preventing the formation of a direct hydrogen bond between O6—H1 and O4. The water molecule also forms a hydrogen bond to O3 of a neighboring FK506 molecule. Another intriguing difference in the crystal structure is the anti orientation about the C25–C26 bond. The orientation is invariably gauche in the 21 other structures, which facilitates the intramolecular hydrogen bonding with O10–H2.

Table III. Intramolecular Hydrogen Bonds in the Structures Found in the Monte Carlo Search[a]

conformation	hydrogen bonds
1	O6—H1···O4; O10—H2···O8
2	O6—H1···O4; O10—H2···O5; O10—H2···O1
3	O6—H1···O4
4	O6—H1···O4; O10—H2···09
5	O6—H1···O4
6	O6—H1···O4; O10—H2···05; O10—H2···O1
7	O6—H1···O4; O10—H2···09
8	O6—H1···O4
9	O6—H1···O4; O10—H2···09
10	O6—H1···O4
11	O6—H1···O4; O10—H2···09
12	O6—H1···O4; O10—H2···08
13	O6—H1···O4; O10—H2···09
14	O6—H1···O4; O10—H2···03; O10—H2···O1
15	O6—H1···O4; O10—H2···01
16	O6—H1···O4; O10—H2···09
17	O6—H1···O4
18	O6—H1···O4; O10—H2···09
19	O6—H1···O4; O10—H2···09
20	O6—H1···O4; O10—H2···09
21	O6—H1···O4; O10—H2···05
X-ray (minimized)	O6—H1···O4

[a] A hydrogen bond is deemed to exist if the distance between the hydrogen and the acceptor is less than 2.5 Å and the donor–hydrogen–acceptor angle is greater than 120°.

Molecular Dynamics

Procedure. In order to investigate the dynamical behavior and solvation of FK506, a molecular dynamics (MD) simulation of the molecule in water was performed. The energy-minimized X-ray structure was taken as the starting point for the MD simulation. This structure was immersed in a box of TIP3P water molecules.[28] Any water molecule with its oxygen atom closer than 1.5 Å or with a hydrogen closer than 0.5 Å to any FK506 atom was removed. Any water molecule with its oxygen farther away than 7.0 Å from any solute atom in the *x*, *y*, or *z* directions was also removed, resulting in a system consisting of the solute

(28) Jorgensen, W. L.; Chandrasekhar, J.; Madura, J. D.; Impey, R. W.; Klein, M. L. *J. Chem. Phys.* **1983**, *79*, 926.

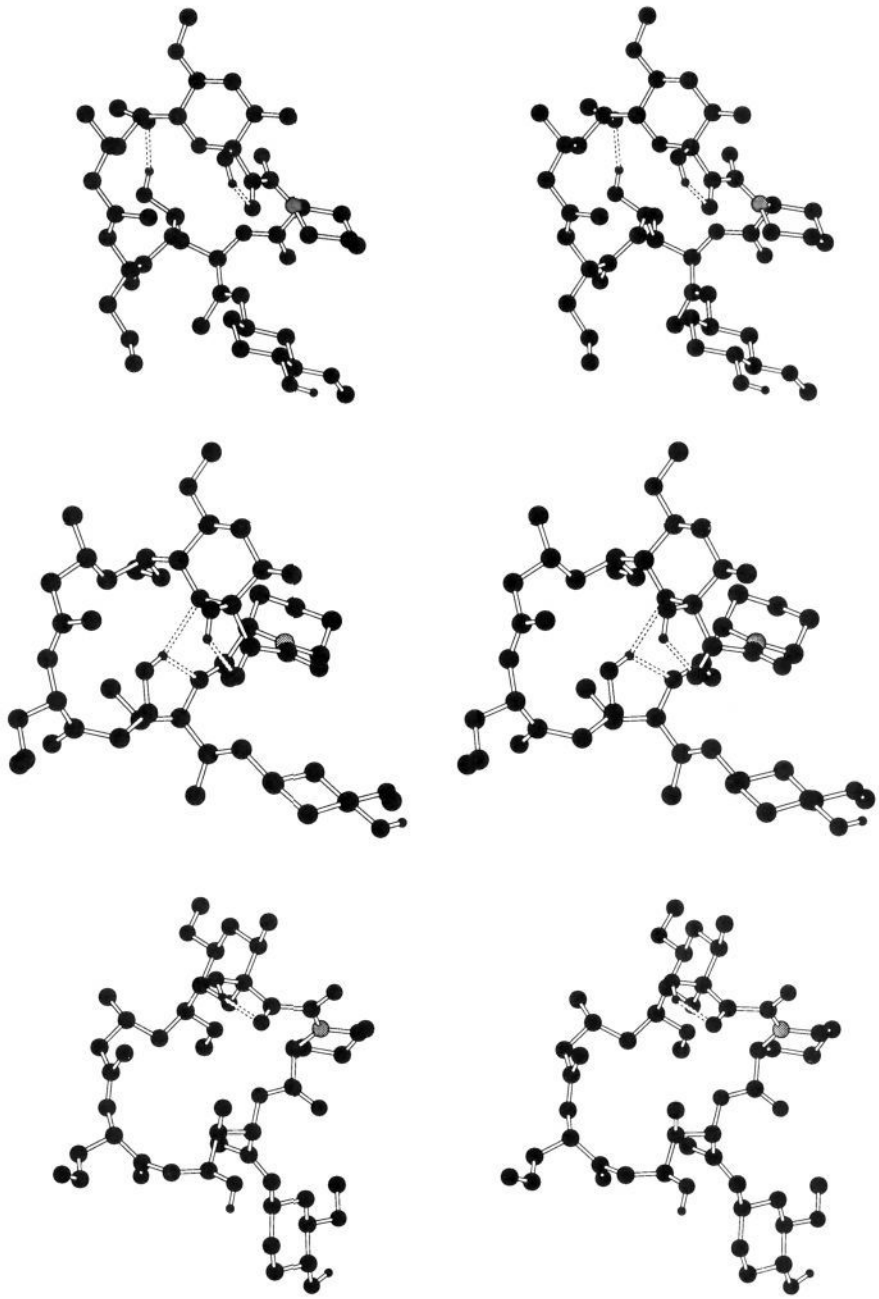

Figure 4. Stereorepresentations of the lowest energy trans (top) and cis (middle) isomers found in the conformational search. The conformation obtained from energy minimization of the crystal structure is shown at the bottom.

and 558 water molecules (1734 total atoms) in a box whose initial dimensions were 28.6 × 28.2 × 21.4 Å. From this point on, periodic boundary conditions were imposed on the system.

Equilibration of the system was achieved in several phases. To begin, the water molecules were energy minimized for 100 steps using a steepest descent algorithm, while keeping the solute geometry fixed. The solvent was then subjected to 5 ps of constant volume dynamics, during which the temperature of the system was raised from 100 to 298 K in a stepwise fashion. An additional 4 ps of simulation followed, keeping the temperature at 298 K, with the solute still fixed. Finally, 1 ps of dynamics was performed in which the solute was allowed to move.

An MD simulation was then performed on this equilibrated system at constant temperature (298 K) and pressure (1 bar = 0.987 atm) for 200 ps. Data analysis was carried out on the entire trajectory; there was no significant transient behavior during the early part of the simulation that might have resulted from imperfect equilibration.

All bond lengths and the H–H distance in water molecules were constrained to their equilibrium values, using the SHAKE algorithm with a tolerance of 0.0004 Å.[29] Nonbonded interactions were calculated using a spherical residue-based cutoff, with FK506 defined as a single residue. The cutoff distance was 9.0 Å. To accelerate the calculations, a nonbonded pair list was used and updated every 10 steps. The time step used in the simulation was 2 fs, and data collection was performed every 0.1 ps. The simulation was performed using AMBER 3.0 Revision A[30] (with local enhancements[31]) on Silicon Graphics 4D workstations.

Conformational Results. Although there are notable conformational changes that occur during the simulation (discussed

(29) van Gunsteren, W. F.; Berendsen, H. J. C. *Mol. Phys.* **1977**, *34*, 1311.
(30) Singh, U. C.; Weiner, P. K.; Caldwell, J.; Kollman, P. A. AMBER 3.0; University of California, San Francisco, CA, 1986. Seibel, G. AMBER 3.0 Revision A; University of California, San Francisco, CA, 1990.
(31) Tirado-Rives, J.; Jorgensen, W. L. *J. Am. Chem. Soc.* **1990**, *112*, 2773. Tirado-Rives, J.; Jorgensen, W. L. *Biochemistry* **1991**, *30*, 3864.

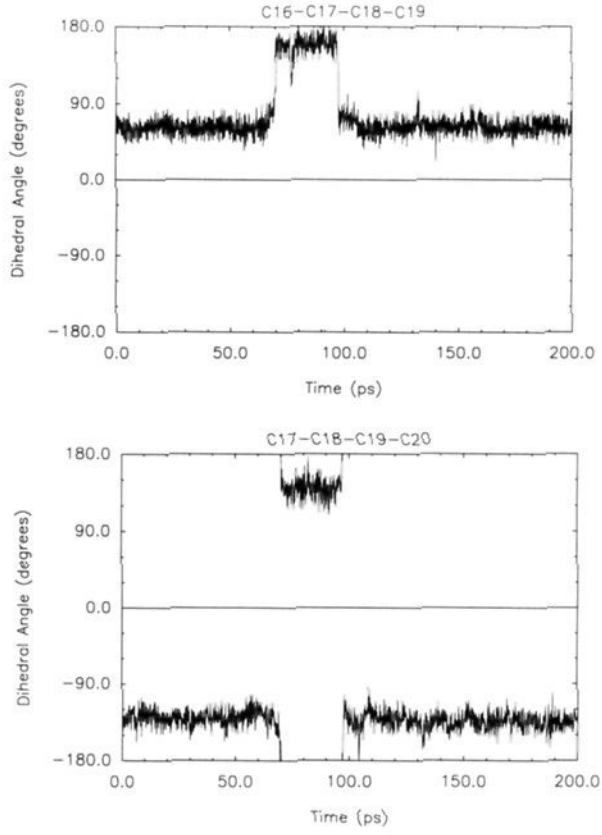

Figure 5. Trajectories of the C17–C18 (top) and C18–C19 (bottom) torsions.

below), the overall shape of the molecule remains essentially the same. The average root mean square deviation of the structures (all atoms) encountered during the simulation (collected at 1-ps intervals) from the actual X-ray crystal structure is 1.04 ± 0.25 Å; the maximum root mean square deviation of any one structure is 1.69 Å.

The average computed values of many dihedral angles of FK506 are shown in Table IV. All three six-membered rings remain in their initial chair conformations with very little fluctuation. The 21-membered macrocycle displays more interesting behavior. Two stable conformations were encountered, the initial one and another during the time interval from 70 to 100 ps. The torsions around the C17–C18 and C18–C19 bonds are primarily responsible. The trajectories of the corresponding dihedral angles are shown in Figure 5. During the 30-ps interval the conformation about the C17–C18 bond is near anti instead of gauche, while the C18–C19 bond has changed skew conformations. Other torsions, while remaining in the same conformation, also reflect some changes, ca. 15–30°, to accommodate this conformational transition: C9–C10, C14–C15, C16–C17, C19–C20 (note this is a double bond), and C21–C22. The structure at 80 ps is representative of the second stable conformation and is shown in Figure 6. In this structure C18 is oriented toward the interior of the macrocycle, whereas in the initial conformation, which may be represented by the minimized X-ray structure (Figure 4, bottom), this atom is oriented outward.

Two other torsions of the macrocycle demonstrate significant flexibility: about C1–C2 and C8–C9 (Figure 7). This is particularly notable since this region is at the binding site of FK506.[11,13] C8–C9 is the α-ketoamide torsion, and C1–C2 is the analogue of the ψ dihedral angle of the homoproline "residue". In spite of their flexibility, however, these two torsions do not sample multiple stable conformations. It should be recalled that these bonds are the ones that show different tendencies in the cis and trans isomers found in the conformational search. The present simulation for the cis isomer shows a preference for maintaining the torsional angle about C8–C9 in the −30° to −120° range. The results from the conformational search (Figure 3) suggest that the trans isomer should show even more flexibility about C8–C9 which may contribute to its preferential binding to FKBP.

In general, the exocyclic torsions are more flexible than the intraring torsions. The fluctuations of the three C–O methoxy group torsions are relatively large, though they remain in their original conformational wells. The three hydroxyl groups show different behaviors (Figure 8). The C10–O6 torsion is comparatively rigid and exists in a single conformation. Motion about C32–O12 is more significant and two staggered minima are sampled. Rotation about C24–O10 is the most facile; several complete rotations occur during the simulation. The different behaviors can be rationalized by considering intramolecular hydrogen bonding (vide infra).

Among the other exocyclic torsions, motion of the cyclohexyl ring around the C28–C29 bond is insignificant during the 200 ps. On the other hand, the smaller allyl group at C21 is relatively mobile. Two stable conformations about the C21–C38 bond are encountered, while several complete rotations occurred around C38–C39 (Figure 9).

Comparison to the X-ray Structure. The structures sampled during the simulation did not drift far from the X-ray structure in view of the maximum root mean square deviation of 1.69 Å. The principal differences are due to the existence of two stable conformations of the macrocycle during the MD simulation and the torsional flexibility for the hydroxyl and allyl groups. Another notable difference is the absence of the intramolecular hydrogen bond between H1 and O4 in the crystal structure.

The fluctuations of the positions of individual atoms during the simulation can be correlated with the crystallographic B factors. The root mean square fluctuation from the MD is simply $\langle \Delta r_i^2 \rangle^{1/2} = \langle (r_i - \langle r_i \rangle)^2 \rangle^{1/2}$, while the B factors can be converted to a comparable quantity using $\langle \Delta r_i^2 \rangle^{1/2} = (3B_i/8\pi^2)^{1/2}$.[32] The

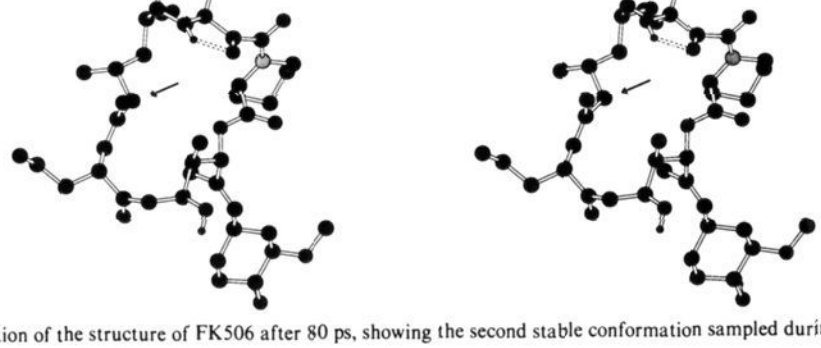

Figure 6. Stereorepresentation of the structure of FK506 after 80 ps, showing the second stable conformation sampled during the MD simulation. The arrow is pointing at C18.

Table IV. Dihedral Angles of FK506 from the MD Simulation and X-ray Structure

torsion	MD av	MD SD	X-ray	torsion	MD av	MD SD	X-ray
			Macrocycle Torsions				
O1-C1-C2-N7	119	30	157	C17-C18-C19-C20[a]	-144	32	-132
C1-C2-N7-C8	-96	9	-96	C18-C19-C20-C21	-178	8	-168
C2-N7-C8-C9	0	11	1	C19-C20-C21-C22	-122	11	-141
N7-C8-C9-C10	-77	17	-95	C20-C21-C22-C23	135	14	137
C8-C9-C10-O5	84	13	90	C21-C22-C23-C24	-126	12	-118
C9-C10-O5-C14	176	6	-177	C22-C23-C24-C25	65	9	59
C10-O5-C14-C15	-177	6	-178	C23-C24-C25-C26	-163	8	-168
O5-C14-C15-C16	73	11	69	C24-C25-C26-O1	179	9	173
C14-C15-C16-C17	61	9	68	C25-C26-O1-C1	153	16	130
C15-C16-C17-C18	-175	12	172	C26-O1-C1-C2	175	11	172
C16-C17-C18-C19[a]	76	34	66				
			Piperidine Torsions				
C2-C3-C4-C5	-53	6	-52	C5-C6-N7-C2	51	8	50
C3-C4-C5-C6	55	6	56	C6-N7-C2-C3	-46	7	-47
C4-C5-C6-N7	-54	6	-53	N7-C2-C3-C4	47	6	47
			Tetrahydropyran Torsions				
C10-C11-C12-C13	-51	6	-55	C13-C14-O5-C10	61	5	59
C11-C12-C13-C14	55	6	58	C14-O5-C10-C11	-58	6	-57
C12-C13-C14-O5	-58	5	-57	O5-C10-C11-C12	51	6	53
			Cyclohexane Torsions				
C29-C30-C31-C32	-57	5	-56	C32-C33-C34-C29	55	6	59
C30-C31-C32-C33	58	6	62	C33-C34-C29-C30	-55	6	-55
C31-C32-C33-C34	-57	5	-62	C34-C29-C30-C31	56	6	54
			Exocyclic Torsions				
C12-C13-O7-C43	83	16	93	C20-C21-C38-C39[a]	-91	44	174
C14-C15-O8-C44	-159	16	-142	C21-C38-C39-C40[b]			130
C30-C31-O11-C45	-75	14	-99	C25-C26-C27-C28	-118	9	-128
C9C10-O6-H1	-4	19	70	C26-C27-C28-C29	-179	7	180
C23-C24-O10-H2[b]			56	C27-C28-C29-C30	118	14	100
C31-C32-O12-H3[a]	34	32	57				

[a] Multiple conformations sampled during MD. [b] Complete rotation encountered during MD.

comparison is shown in Table V and Figure 10. The qualitative accord is significant in view of the difference between the crystalline and solution environments.

It is possible to rationalize some of these data. Both the MD and X-ray results show relatively large fluctuations for C4 and C5, which are on the outside of the piperidine ring. As mentioned above, motion about C1–C2 and C8–C9 torsions is relatively facile, and these torsions certainly play a role in determining the position of the piperidine ring. The flexibility is enhanced in solution compared to the crystal and yields greater motion for C4 and C5. Also related to the flexibility of the C8–C9 torsion is the large fluctuation observed for O3.

The MD results predict a large fluctuation for C18. This is attributable to the two conformations that are sampled for the dihedral angles flanking this atom. A large fluctuation is also calculated for C36, which is the methyl group attached to C17, presumably for the same reason.

C12, C35, and O7 also show relatively large fluctuations in the MD simulation. These atoms are on the periphery of the tetrahydropyran ring. A possible explanation is that the two torsions defining the position of this small ring relative to the macrocycle are about C9–C10 and C14–C15, which are two of the secondary torsions involved in the conformational change of the macrocycle. Although the changes in these torsions are small, C12, C35, and O7 are located on the outside edge of the ring and would be expected to show the largest fluctuations.

The relatively large fluctuations for C32 (in the X-ray results) and C33 (in the MD) are probably due to their location on the cyclohexane ring. What is surprising is that their fluctuations are not bigger; this indicates that the C28–C29 linkage is really quite rigid. Not surprisingly, the largest fluctuation in both the X-ray and MD results is for C40, which is the terminus of the rapidly rotating allyl group.

(32) Willis, B. T. M.; Pryor, A. W. *Thermal Vibrations in Crystallography*; Cambridge University Press: Cambridge, England, 1975.

Table V. Root Mean Square Fluctations (Å) from the MD Simulation and X-ray Structure

atom	MD	X-ray	atom	MD	X-ray
C1	0.396	0.455	C30	0.346	0.559
C2	0.404	0.461	C31	0.406	0.623
C3	0.859	0.556	C32	0.546	0.662
C4	1.089	0.656	C33	0.701	0.598
C5	1.089	1.681	C34	0.631	0.512
C6	0.831	0.627	C35	0.851	0.520
N7	0.507	0.517	C36	0.785	0.505
C8	0.567	0.516	C37	0.662	0.691
C9	0.477	0.485	C38	0.638	0.634
C10	0.380	0.446	C39	1.018	0.715
C11	0.499	0.445	C40	1.272	0.943
C12	0.604	0.467	C41	0.526	0.505
C13	0.553	0.445	C42	0.617	0.520
C14	0.273	0.424	C43	1.198	0.692
C15	0.362	0.449	C44	1.117	0.736
C16	0.438	0.450	C45	1.040	0.682
C17	0.510	0.434	O1	0.391	0.464
C18	0.869	0.478	O2	0.698	0.566
C19	0.536	0.481	O3	0.919	0.662
C20	0.423	0.456	O4	0.731	0.567
C21	0.327	0.477	O5	0.262	0.431
C22	0.360	0.446	O6	0.741	0.488
C23	0.424	0.465	O7	0.867	0.531
C24	0.438	0.428	O8	0.802	0.511
C25	0.352	0.430	O9	0.629	0.495
C26	0.336	0.434	O10	0.694	0.477
C27	0.298	0.450	O11	0.688	0.821
C28	0.311	0.461	O12	0.696	0.803
C29	0.292	0.485			

C43, C44, and C45 as well as O7, O8, and O11 are associated with the methoxy groups. They are relatively more mobile than the atoms in the macrocycle. Once again, the flexibility is enhanced in solution.

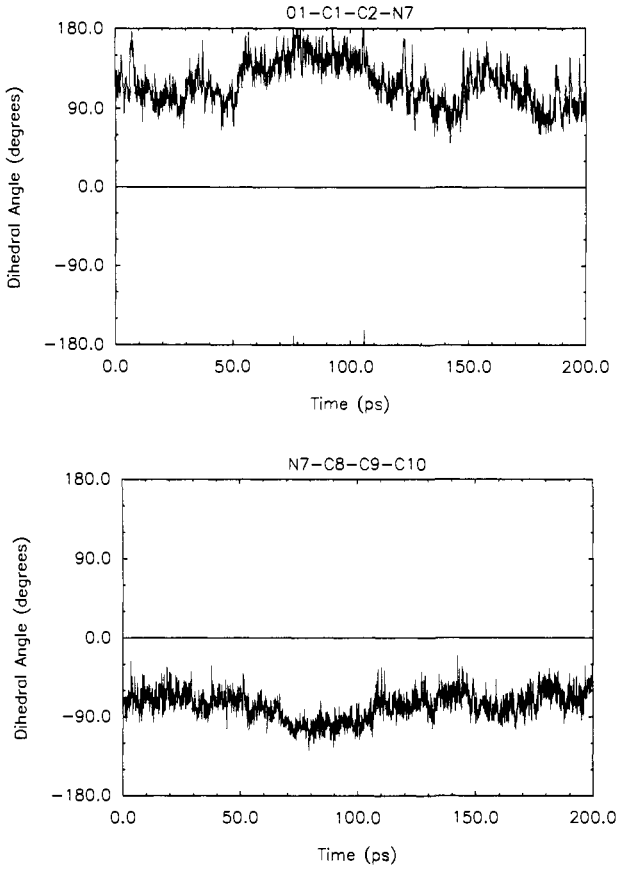

Figure 7. Trajectories of the C1–C2 (top) and C8–C9 (bottom) torsions.

Comparison to the NMR Structure. Kessler and co-workers have used the NMR spectra of FK506 in $CDCl_3$ and restrained molecular dynamics to obtain solution structures of the cis and trans isomers.[10] There were notable differences in the C21–C26 region between the X-ray crystal structure and the proposed solution structure of the cis isomer. The present simulation, which used no experimental constraints, does not show such deviations from the crystal structure, though only 200 ps have been covered. There *is* a deviation in the position of C18, which is caused by the multiple conformations about the C17–C18 and C18–C19 bonds. It appears that the difference between the NMR and crystal structures is also attributable to the presence of multiple conformations. In the NMR structure the standard deviations of the dihedral angles in the region in question are particularly large, comparable to what is found in the present simulations when multiple conformations are involved (Table IV).

It is interesting that the NMR structure for the trans isomer also has large deviations for the dihedral angles in the same region. It may be noted that the proposed trans structure does not correspond to any structure found during the conformational search described above.

Hydrogen Bonding. In defining hydrogen bonds, a purely geometric criterion was used. A hydrogen bond is deemed to exist if the distance between the hydrogen and the acceptor is less than 2.5 Å, and the donor–hydrogen–acceptor angle is greater than 120°. On the basis of this criterion, the occurrences of hydrogen bonds during the MD simulation are shown in Table VI.

Two intramolecular hydrogen bonds are found. The hydrogen bond O6—H1···O4 is not observed in the crystal structure, but is formed upon the initial minimization. During the simulation, this hydrogen bond is present about half of the time. Another evidence of its existence is the relatively small fluctuations of the dihedral angle about C10–O6, compared to the other hydroxyl group (Figure 8).

The second intramolecular hydrogen bond, O12—H3···O11, is transitory at best. It is seen only 18% of the time. However, it does put *some* restraint on the torsion about C32–O12, as compared to the most flexible hydroxyl torsion (C24–O10).

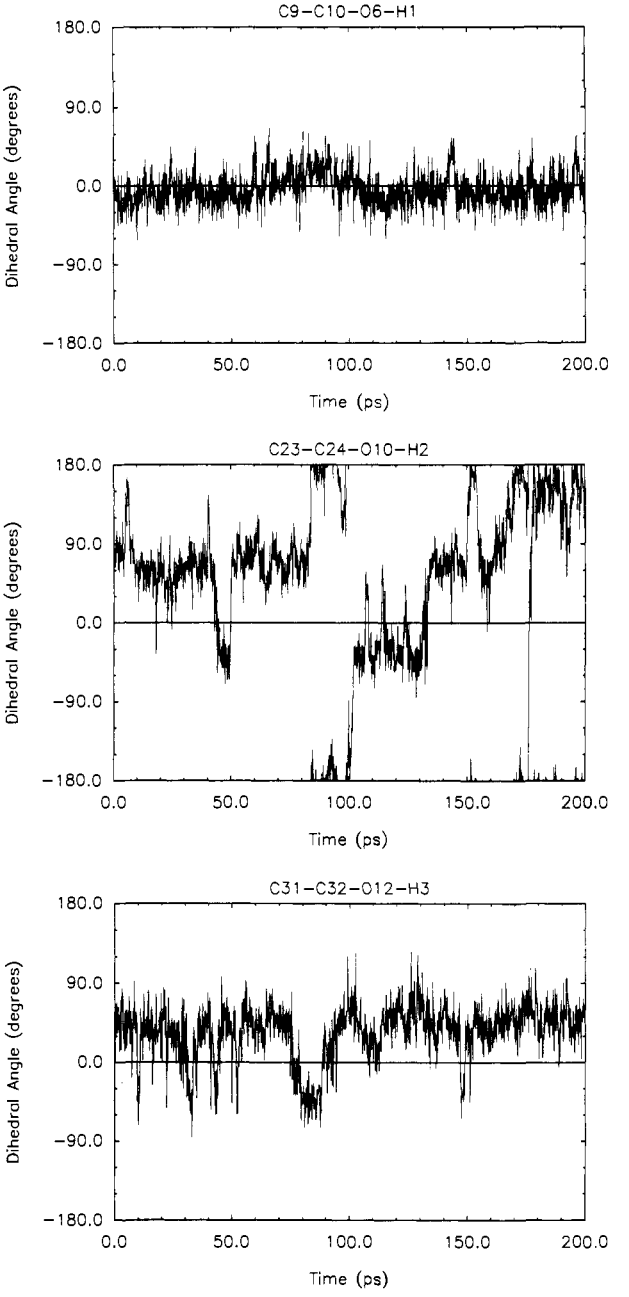

Figure 8. Trajectories of the three hydroxyl group torsions: C10–O6 (top), C24–O10 (middle), and C32–O12 (bottom).

Table VI. Hydrogen Bond Occurrences[a]

donor	acceptor	freq	donor	acceptor	freq
		Intramolecular			
O6	O4	1241	O12	O11	364
		Intermolecular			
O6	water	1102	O12	water	1819
O10	water	2143			
water	N7	90	water	O7	1906
water	O1	16	water	O8	631
water	O2	2262	water	O9	2826
water	O3	3263	water	O10	2945
water	O4	1450	water	O11	1820
water	O5	129	water	O12	3791
water	O6	2049			

[a] Out of 2000 configurations saved during the MD.

The hydrogen bonding between FK506 and the solvent has also been monitored. Each hydroxyl group can act as a donor, and

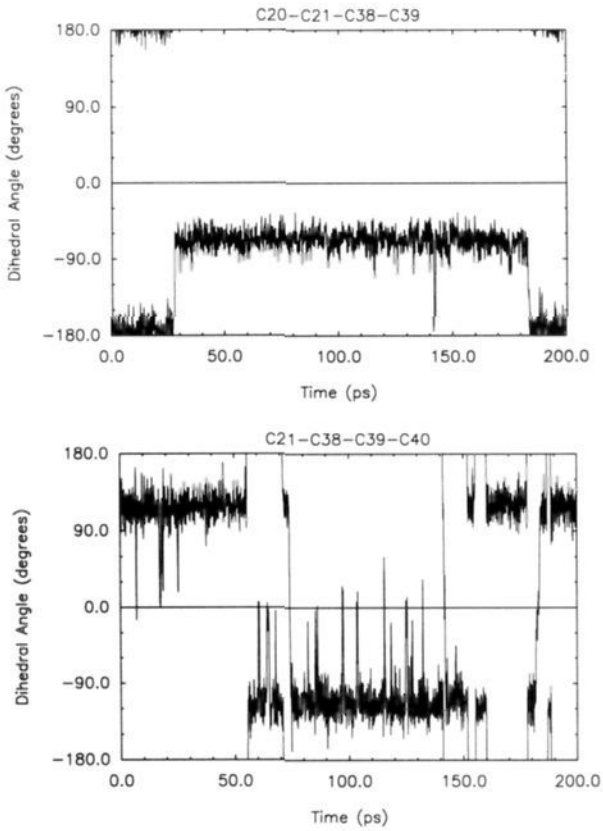

Figure 9. Trajectories of the allyl group torsions: C21–C38 (top) and C38–C39 (bottom).

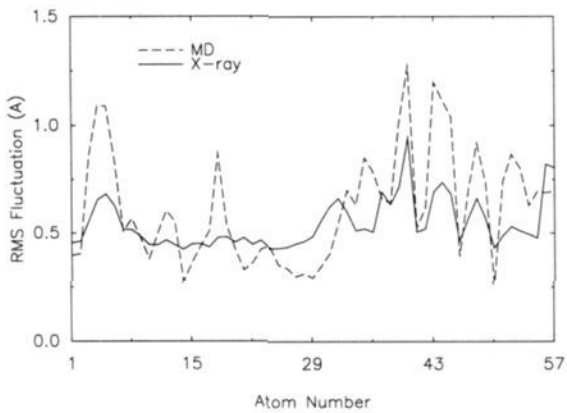

Figure 10. Positional fluctuations of the heavy atoms from the MD simulation and the X-ray *B* factors. Atom numbers correspond to the order in Table V.

on average forms one hydrogen bond in this mode. For O10–H2 the hydrogen bond is always intermolecular. O6–H1 acts as an intermolecular hydrogen-bond donor only about half the time, because the rest of the time it is involved in the intramolecular hydrogen bond to O4. Similarly, O12–H3 acts as an intermolecular hydrogen-bond donor somewhat less than 100% of the time, since it is occasionally intramolecularly hydrogen bonded to O11. The hydroxyl group oxygens are also found to act as hydrogen bond acceptors for 1–2 water molecules; the lowest frequency is for O6 which is partially shielded by the tetrahydropyran ring as seen in Figure 11.

Some other potential acceptors are obviously buried in the interior of the molecule (N7, O1, O5), and they hardly participate in hydrogen bonding. Among the methoxy group oxygens, O8 is rarely involved in a hydrogen bond. An explanation is apparent upon inspection of the structures generated during the simulation, e.g., Figure 11. O8 is turned inward toward the center of the macrocycle and C44 is oriented outward. Across from O8 are the ester group and the cyclohexyl appendage. These groups sterically interfere with approaching water molecules. Thus, O8 is not as exposed to the solvent as one might think and is not effectively acting as a hydrogen bond acceptor. Rotation to permit hydrogen bonding to O8 may cause steric clashes between C44 and the macrocycle. However, the other methoxy oxygens, O7 and O11, are more on the periphery of FK506 and participate in an average of one hydrogen bond with water.

Turning to the four carbonyl oxygens, O4 shows the lowest frequency of hydrogen bonding with water. This results from its inward orientation toward the macrocycle and its intramolecular hydrogen bond with O6–H1. The other carbonyl oxygen in the critical binding region, O3, is oriented outward in the X-ray structure as well as in the 21 optimized structures. Solvent exposure is not complete in view of the proximity of the piperidine ring and the C35 methyl group; however, O3 manages to participate in an average of 1.6 hydrogen bonds with water molecules. The ester oxygen, O2, has about one hydrogen-bonded water molecule. It is more exposed than O4, though it is partially shielded by the piperidine ring. Finally, the keto oxygen, O9, is directed inward, but is still relatively exposed, and participates in an average of 1.4 hydrogen bonds. In summary, it may be noted from Table VI that in the C1–C10 binding region there are an average of 5 hydrogen bonds between water molecules and the cis isomer of FK506. It would be interesting to discern differences in the hydration of the cis and trans isomers that might contribute to the preferential binding of the trans form.

Figure 11 shows the final structure of FK506 after 200 ps of MD simulation. It is notable that most of the analysis above, based on averaging over the entire 200-ps trajectory, remains valid even for this instantaneous structure. The least accessible potential acceptors (N7, O1, O5, O8) have no hydrogen bonds. The other acceptors generally have one hydrogen-bonded water molecule, except for O10, which has 3 (on average, 1.5 are found), O2, which has 2 (expected, 1), and O7 and O4, which have none (expected,

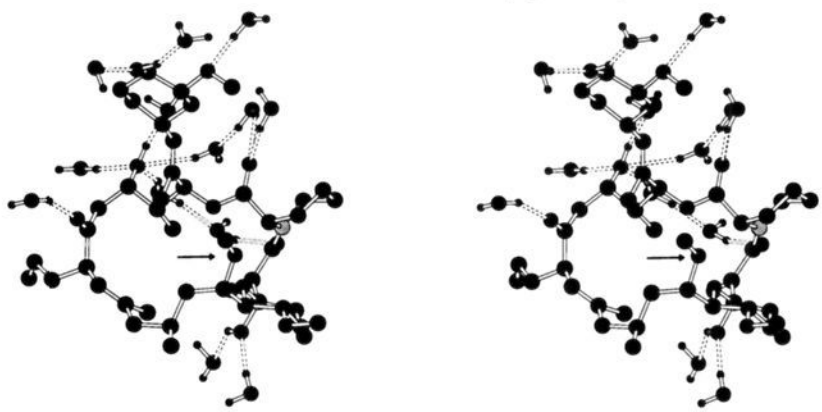

Figure 11. Stereorepresentation of the structure of FK506 after 200 ps of MD simulation. The binding region is to the right and O8 is indicated by the arrow. The hydrogen-bonded water molecules are also shown.

1 and 0.5, respectively). Also noteworthy is that in this structure O6-H1 is hydrogen bonded to a solvent molecule instead of to O4. The other hydroxyls are also hydrogen bonded to water molecules, as expected. In the binding region, 5 hydrogen-bonded water molecules are observed (2 to O2, 1 to O3, 2 to O6-H1), consistent with the analysis above.

Conclusions

Conformational searching of FK506 in isolation revealed the existence of a large number of low-lying energy minima. Both cis and trans amide isomers are found among these minima and appear to favor different conformations of nearby torsions. Since two of these torsions, about C1-C2 and C8-C9, are in the binding region of FK506, these preferences may be relevant to the preferential binding of the trans isomer to FKBP.

Molecular dynamics simulation in water over 200 ps revealed some interesting conformational behavior. Notable observations are the flexibility of the binding region of FK506 and the sampling of two conformations of the macrocyclic ring. The solution structure, as obtained from the simulation, correlates well with the X-ray crystal structure, even to the extent of positional fluctuations of the individual atoms. Hydration of FK506, as analyzed through hydrogen bonding, reflects significant variations in the exposure of potential hydrogen-bonding sites. There are on average 5 hydrogen bonds between water molecules and FK506 in the critical binding region.

Acknowledgment. Gratitude is expressed to the National Institutes of Health for support of this work. We also thank Dr. Julian Tirado-Rives for computational assistance and Professor Stuart L. Schreiber for valuable discussions.

Registry No. FK506, 104987-11-3.

Supplementary Material Available: Complete listing of AMBER parameters for FK506 and stereopictures and tables of coordinates of the structures found in the conformational search (25 pages). Ordering information is given on any current masthead page.

Elucidation of Solution Structures by Conformer Population Analysis of NOE Data

Clark Landis* and Viyola S. Allured†

Contribution from the Department of Chemistry, University of Wisconsin, Madison, Wisconsin 53705, and the Department of Chemistry and Biochemistry, University of Colorado, Boulder, Colorado 80309. *Received June 14, 1991*

Abstract: The elucidation of molecular structures from NOE data may be complicated by the presence of multiple solution conformations. Conformer population analysis (CPA) is a new procedure for obtaining solution structures from NOE data that accommodates multiple conformations and avoids some of the biases inherent in the construction of single structures from NOE distance matrices. The CPA method utilizes trial conformers generated by molecular modeling techniques and solves for the set of conformer populations that yield the most significant best-fit to the NOE data. Simulations of transient NOE experiments and steady state NOE experiments illustrate the method and the factors that influence the qualities of the results.

I. Introduction

NMR methods for the elucidation of molecular structures in solution[1] are popular and powerful because the methods do not require special molecular properties (such as single-crystal growth required by crystallography or significant vapor pressures as required for electron-diffraction work) and because the methods probe the structure in the liquid phase, the most common reaction medium. These methods have been applied extensively to the determination of peptides and small proteins.

Structural information arises from NMR experiments of two types: the NOE-based techniques (NOESY,[2] ROESY,[3] and related methods[4]), which express internuclear distance information, and scalar coupling measurements,[5] which are sensitive to torsion angles. Whereas the scalar coupling measurements yield information about the local structure, the NOE-based methods uniquely reveal gross (tertiary) structural features in addition to local features. Thus, modern NMR methods for protein sequencing and the determination of secondary and tertiary structure strongly emphasize ^{1}H NOE measurements.[1]

The interpretation of NOE information commonly follows one of two courses:[6] (1) a "best-fit" approach or (2) a molecular construction approach. The former viewpoint employs a predefined collection of different structural possibilities, or conformers, and seeks to distinguish which structures are consistent, either collectively or individually, with the NMR data. For this approach the NOE intensities of individual, predefined conformers are computed and then compared with observed intensities. The most elaborate applications of this approach attempt to maximize the fit of observed and calculated NOE intensities by varying the populations of the conformers. A disadvantage of this method

* University of Wisconsin.
† University of Colorado.

(1) (a) Wutrich, K. *Acc. Chem. Res.* **1989**, *22*, 36. (b) Wutrich, K. *NMR of Proteins and Nucleic Acids*; Wiley: New York, 1986.
(2) Jeener, J.; Meier, B. H.; Bachmann, P.; Ernst, R. R. *J. Chem. Phys.* **1979**, *71*, 4546-4553.
(3) (a) Bothner-By, A. A.; Stephens, R. L.; Lee, J.; Warren, C. D.; Jeauloz, R. W. *J. Am. Chem. Soc.* **1984**, *106*, 811-813. (b) Bax, A.; Davis, D. G. *J. Magn. Reson.* **1986**, *68*, 568-574. (c) Kessler, H.; Griesinger, C.; Kerssebaum, R.; Wagner, K.; Ernst, R. R. *J. Am. Chem. Soc.* **1987**, *109*, 607-609. (d) Griesinger, C.; Ernst, R. R. *J. Magn. Reson.* **1987**, *75*, 261-271.
(4) (a) Dobson, C. M.; Olejniczak, E. T.; Poulsen, F. M.; Ratcliff, R. G. *J. Magn. Reson.* **1982**, *48*, 97. (b) Bother-By, A. A.; Noggle, J. H. *J. Am. Chem. Soc.* **1979**, *101*, 5152. (c) Kessler, H.; Oschkinat, H.; Griesinger, C.; Bermel, W. *J. Magn. Reson.* **1986**, *70*, 106-133. (d) Williamson, M. P.; Neuhaus, D. *J. Magn. Reson.* **1987**, *72*, 369. (e) Noggle, J. H.; Schirmer, R. E. *The Nuclear Overhauser Effect*; Academic Press: New York, 1971.
(5) (a) Bystrov, V. F. *Prog. Nucl. Magn. Reson. Spectrosc.* **1976**, *10*, 41-81. (b) Pardi, A.; Billeter, M.; Wurtrich, K. *J. Mol. Biol.* **1984**, *180*, 741. (c) Haasnoot, C. A. G.; DeLeeuw, F. A. A. M.; Altona, C. *Tetrahedron* **1980**, *36*, 2783.
(6) Williamson, M. P.; Neuhaus, D. *The Nuclear Overhauser Effect in Structural and Conformational Analysis*; VCH: New York, 1989.

0002-7863/91/1513-9493$02.50/0